Observation of the $A^2\Sigma^+ \leftarrow X^2\Pi$ Electronic Transition of NaO§

S. Joo,‡ D. R. Worsnop,*,† C. E. Kolb,*,† S. K. Kim,‡,|| and D. R. Herschbach*,‡

Center for Cloud and Aerosol Chemistry, Aerodyne Research, Inc., Billerica, Massachusetts 01821-3976, and Department of Chemistry and Chemical Biology, Harvard University, Cambridge, Massachusetts 02138

Received: March 2, 1999

The gas-phase infrared spectrum of the $A^2\Sigma^+ \leftarrow X^2\Pi$ electronic transition of the NaO radical was observed for the first time utilizing tunable diode laser differential absorption spectroscopy; 109 lines were found within the region 2015−2095 cm^{-1} and 45 lines within 2654−2696 cm^{-1}. The NaO radical was produced by reaction of sodium vapor with N_2O in a fast flow tube and detected using an astigmatic Herriott multipass absorption cell combined with rapid sweep integration absorption signal processing. Simple kinetic studies were performed in order to differentiate the NaO radical features from precursor N_2O lines. The NaO $A^2\Sigma^+ \leftarrow X^2\Pi$ vibronic band structure was modeled using ab initio calculations by Langhoff and co-workers; the simulated NaO band profile agrees reasonably well with that observed. A preliminary assignment of some observed lines and the resulting molecular constants are presented. Quantitative absorption strength measurements indicate that either absorption line strengths for this transition are significantly smaller than indicated by ab initio calculations or the Na + N_2O reaction produces a significant fraction of NaO(A) state which resists collisional quenching under our experimental conditions.

Introduction

In 1939, Chapman proposed a two-step reaction sequence to explain the Na D-line nightglow in the mesosphere.[1] He suggested that Na ablated from meteors reacted with O_3 to form NaO, which then reacted with O to reform Na atoms, some of them electronically excited. In 1976, Kolb and Elgin pointed out that reactions between Na and O_3 and between NaO and O should proceed by fast electron-jump processes.[2] That allows the Chapman reaction scheme to account for both the observed ambient Na night glow and the persistent visible trails left by large meteors, provided that the production of excited Na(^{2}P) atoms in the second step is efficient. A symmetry correlation analysis of the reaction between ground-state NaO($X^2\Pi$) and ground-state O(^{3}P) by Bates and Ojha[3] suggested that the branching ratio to form Na(^{2}P) indeed could be as large as $f = 0.33$.

However, in 1986, contrary evidence appeared. Plane and Husain[4] carried out a flash photolysis kinetic study of NaO + O(^{3}P) in an atmospheric pressure heat pipe and found $f < 0.01$, although the rate constant was near gas kinetic (as predicted[2]). The analysis of this experiment has been questioned by Schofield.[5,6] Yet current models of mesospheric chemistry require $f \sim 0.1$ to match observed Na nightglow levels,[7,8] and it seems very unlikely that the upper limit for f obtained by Plane and Husain is sufficiently in error to be consistent with such a large branching ratio. Since, in their atmospheric pressure experiment, collisional relaxation would ensure that the NaO would be almost solely in the $X^2\Pi$ ground electronic state, the question arose whether the mesospheric reaction might involve instead NaO in the low-lying excited $A^2\Sigma^+$ state.

This prompted a molecular beam magnetic deflection analysis of NaO formed from the Na + O_3 reaction,[9] which showed that in fact the NaO radical is predominantly produced in the excited $A^2\Sigma^+$ state. Photoelectron spectroscopy by Wright, Ellis, and Dyke[10] likewise found Na + O_3 at low pressures gave NaO($A^2\Sigma^+$) as the major product. Furthermore, a symmetry correlation analysis of the NaO($A^2\Sigma^+$) + O(^{3}P) reaction[11] showed that two-thirds of the allowed pathways via energetically accessible doublet states correlate with an excited Na(^{2}P) atom, indicating a large value of f for this reaction. The analysis also showed that if implausible pathways via quartet states are omitted, the large f predicted by Bates and Ojha for NaO($X^2\Pi$) + O(^{3}P) would vanish, in accord with the experiment of Plane and Husain. These results indicate that if the Chapman mechanism is to explain the mesospheric Na nightglow, it must involve NaO($A^2\Sigma^+$).

There is no previous experimental information on the NaO($A^2\Sigma^+$) state, and even for the ground state it is sparse. Ab initio calculations[12−16] have predicted the energy separation between the $^2\Pi$ and $A^2\Sigma^+$ states of NaO to be in the range $\Delta = 1431-2117$ cm^{-1}. The lambda-doubling constant obtained from the NaO($X^2\Pi$) microwave spectrum,[17] if interpreted using pure precession theory, indicates $\Delta \sim 2050$ cm^{-1}. The transition dipole moment for the $A \leftarrow X$ transition of NaO has been calculated to be less than 0.2 D.[16,17] For the $X^2\Pi$ state, the microwave spectrum has provided structural parameters and hyperfine constants.[17] The adiabatic ionization energy of NaO has been determined from photoelectron spectroscopy.[10] Chemiluminescence[18] and laser-induced fluorescence spectra[19] of NaO visible transitions have also been reported.

In this work, infrared tunable diode laser differential absorption measurements of NaO have revealed a rich spectrum, the first observation of the $A \leftarrow X$ vibronic transitions. In the regions 2015−2095 and 2654−2695 cm^{-1}, a total of 154 lines were recorded. The NaO radical was generated in a fast flow reactor by the reaction of Na + N_2O and probed in a novel astigmatic

§ Dedicated to Sidney W. Benson in honor of his 80th birthday.

* Corresponding authors: worsnop@aerodyne.com, kolb@aerodyne.com, fax 978-663-4918; hbach@chemistry.harvard.edu, fax 617-495-4723.

† Aerodyne Research, Inc.

‡ Harvard University.

|| Permanent address: Department of Chemistry, Seoul National University, Seoul 151-742, Korea.

10.1021/jp990741q CCC: $18.00
Published on Web 04/08/1999

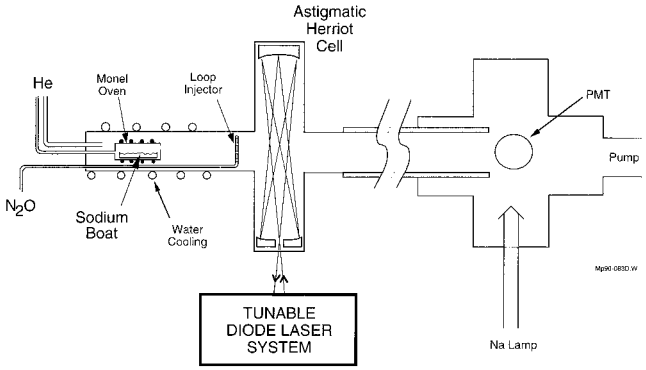

Figure 1. Fast flow reactor for NaO kinetics and spectroscopy.

Herriott multiple pass absorption cell. The observed spectrum has been simulated with an analysis program based on the calculations of Langhoff et al.[15,16] The comparison between the observation and simulation was best matched by shifting Langhoff's predicted band origin to higher frequency by 75 cm^{-1}. Atomic sodium decay and NaO signal intensity were monitored as a function of N_2O concentration. Observed spin-rotation doublet splittings due to magnetic interactions were also a diagnostic for NaO transitions. We present preliminary line assignments and derived $A^2\Sigma^+$ state molecular constants and discuss the impact of these results on our understanding of the mesospheric sodium nightglow.

This work is dedicated to Sidney W. Benson in honor of his 80th birthday; he has long been interested in mesospheric sodium compounds and has contributed insightful studies of their fate after they reach stratospheric altitudes. [20,21]

Experimental Section

Figure 1 shows the fast flow reactor used to produce NaO radicals. The setup is similar to a system previously employed to measure the kinetics of reactions between Na and O_3 or N_2O.[22] Sodium vapor emerges from a monel oven and reacts with N_2O gas injected ~7 cm downstream of the oven. About 15 cm downstream of the oven the flowtube was fitted with a glass cross containing a Herriott multipass cell coupled to a tunable diode laser (TDL) used to observe the NaO spectrum. At the end of the reactor, about 90 cm further downstream, Na vapor density was monitored via resonance fluorescence, excited by a hollow cathode sodium lamp, and observed with a photomultiplier tube mounted perpendicular to the lamp beam.

In typical runs, helium or argon carrier gas was introduced at the entrance of the reactor, with the flow rate (monitored with a Matheson meter) set to maintain the total pressure at 1−3 Torr (measured with a MKS Baratron capacitance manometer). The monel oven, containing about 1 g of metallic sodium in a silver boat, was heated to 320−420 °C by a ceramic heater. A jacket around the oven and the neighboring segment of the flowtube were cooled by circulating water. The temperature of the flow reactor was monitored with a thermocouple attached to its outer wall. Argon (at 18−30% of the total gas flow) was injected in the arms of the Herriott cell to provide a buffer gas to protect the mirrors. Gas flows, including reaction products, were pumped out continuously with a roots blower.

Na vapor pressure within the oven of 10^{-5}−10^{-3} Torr was diluted in the reactor by the carrier gas and further reduced by loss to the walls. N_2O reactant was introduced into the flow tube through a looped Pyrex injector. N_2O and Ar were alternated through the injector with a cycle time of 0.1 to ~5 s by switching a solenoid valve, to enable background subtraction for the TDL spectroscopy. Although the NaO concentration could not be directly determined, the production of NaO was readily apparent from the conversion of Na depositions on the reaction zone walls from 'silver' to 'white'. The reaction of Na was also consistent with N_2O reaction kinetics as monitored by loss of atomic Na signal at the resonance fluorescence detector at the end of the reactor.

TABLE 1: Parameters for Simulation of Vibronic Bands[a]

band $\nu_A' - \nu_X''$	origin, cm^{-1}	$A_{\nu'\nu''}$, s^{-1}	band $\nu_A' - \nu_X''$	origin, cm^{-1}	$A_{\nu'\nu''}$, s^{-1}
0−0	1918.56	56.0	2−1	2440.24	119
1−0	2417.47	108	3−1	2924.94	138
2−0	2908.48	62.3	1−2	1485.48	9.25
0−1	1450.31	11.3	3−2	2461.19	92.3
1−1	1949.22	7.15	4−2	2940.12	203

[a] From ref 16.

The Herriott absorption cell was configured for 54 passes on a 32 cm base path based on an astigmatic mirror design.[23] The TDL optical system includes a co-aligned HeNe laser beam to aid coupling the infrared laser through the multipass cell onto the detector (Santa Barbara Research InSb). The NaO flow is estimated to be about 2−4 cm wide in the center of the flow tube, limited by mixing of the N_2O and purge Ar flows from the arms of the cell, giving an effective absorption path length of ~100−200 cm. Light exiting the Herriott cell could be passed through a grating monochromator (kinematically demountable) to check laser mode frequency and purity.[24] A computerized data acquisition system signal averaged fast sweeping (~1 kHz) of diode current to give digitized absorption spectra containing 300−1000 points. Automated background subtraction (via switching N_2O on and off) and nonlinear fitting of absorption line profiles, together with laser baseline and tuning rates, gave a sensitivity of $\sim 10^{-5}$ in $\Delta I/I$ absorption.

Six diode lasers (Laser Photonics) were used to scan the wavenumber regions of 1981.5−2096.5, 2645.7−2697.1, and 2840−2956.1 cm^{-1} (see Appendix). Each diode laser could be tuned over 100−150 cm^{-1} with approximately 30−35% coverage of the tuned range, the gaps resulting from hopping between laser modes. Laser modes were tuned by carefully controlling the cryostat temperature (30−70 K) and scanning laser current. Laser intensity was monitored by electronically switching off the laser during a portion of the computer-controlled sweep. Precise laser frequencies were determined by recording reference absorptions of OCS and CH_4 in a static gas cell (10 cm), depending on the frequency region. The accuracy of the frequency determination was estimated to be better than ~0.005 cm^{-1} in most cases. Although at our low pressures of 1−3 Torr the line shape should be a Gaussian due to Doppler broadening, because of jitter in the diode laser frequency, it was considered more appropriate to fit spectral lines to a Voigt profile.

Simulated Spectrum. Before searching experimentally for the $A^2\Sigma^+ \leftarrow X^2\Pi$ spectrum of NaO, we computed band profiles, using parameters obtained from the ab initio electronic structure calculations of Langhoff et al.[15,16] and from the microwave spectrum of the $X^2\Pi$ state.[17] The 10 strongest vibronic bands were simulated, with $\nu_A - \nu_X$ = 0−0, 1−0, 2−0, 0−1, 1−1, 2−1, 3−1, 1−2, 3−2, 4−2.

Transition Frequencies. The rovibronic transition frequencies were obtained by adding the differences between the A and X state rotational terms to the calculated vibronic band origins. The parameters used are listed in Tables 1 and 2. The rotational structure is complex due to the presence of both electronic orbital and spin angular momentum. An energy level diagram indicating the allowed transitions for a $^2\Pi - ^2\Sigma^+$ band

TABLE 2: Parameters for Simulation of Rotational Structure[a]

quantity	$\nu = 0$	$\nu = 1$	$\nu = 2$
	Ground State, X^2P		
B''	0.422	0.418	0.414
p''	0.044	0.047	0.052
q''	0.00031	0.00033	0.00036
A''_{so}	−107	(−107)	(−107)
	Excited State, $A^2\Sigma^+$		
B'	0.465	0.460	0.456
γ'	(0.01)	(0.01)	(0.01)

[a] In cm^{-1} units. For X state, rotational constant B″, lambda-doubling parameters p'' and q'', and spin−orbit coupling constant A''_{so} are from ref 17. For A state, B' is from multireference configuration interaction calculations of ref 15 and spin-rotation constant γ' is a nominal estimate.

TABLE 3: Observed NaO Absorption Lines, $\Delta v = 0$ Band[a]

frequency	absorbance[b]	frequency	absorbance[b]	frequency	absorbance[b]
2015.440	4.12	2052.728	14.9	2071.867	2.86
15.447	4.12	52.824	20.0	72.717	15.3
23.289	2.67	52.915	4.68	72.810	6.83
23.377	3.40	53.034	12.1	73.010	6.64
27.470	2.26	53.290	20.0	75.739	2.91
27.529	2.50	53.402	6.81	2076.255	8.17
36.302	7.18	53.524	16.6	76.825	8.94
36.308	7.18	56.261	11.1	76.905	6.38
39.158	3.91	56.512	11.4	78.404	6.52
39.170	3.91	56.884	19.0	78.487	9.19
39.226	3.83	57.205	12.9	78.721	4.60
39.556	2.55	57.435	5.11	2079.013	11.0
44.841	13.8	57.597	2.38	79.086	6.55
45.005	15.8	57.711	9.53	79.867	9.79
45.280	8.17	59.387	7.23	80.002	7.61
45.404	3.91	59.978	3.61	83.280	12.6
45.499	10.2	60.041	2.57	83.504	2.43
45.801	3.23	60.089	13.1	83.680	13.8
45.829	3.40	60.369	1.84	83.735	8.14
46.109	3.74	60.412	5.14	83.982	6.88
47.899	3.20	60.616	6.89	85.807	6.38
48.507	7.51	60.846	3.29	86.149	4.68
48.752	4.26	61.341	5.75	86.194	3.40
49.489	12.3	64.129	13.8	86.278	2.81
49.669	4.00	64.135	7.66	86.304	2.55
49.957	16.0	64.633	4.97	87.568	5.11
50.034	6.66	66.898	4.31	87.628	4.09
50.059	8.00	67.360	5.87	88.115	3.83
50.097	3.00	67.388	3.83	88.160	2.81
50.198	7.00	68.120	4.09	91.197	7.88
50.248	8.36	68.291	13.8	91.388	7.42
51.086	12.0	68.783	5.11	91.405	6.45
51.396	20.0	68.913	5.11	95.007	3.46
51.679	10.0	69.093	5.11	95.168	4.95
52.044	17.8	71.012	4.27	95.329	3.10
52.106	17.8	71.616	5.55	95.418	3.25
52.432	17.0				

[a] For $A^2\Sigma^+ \leftarrow X^2\Pi$, $v'-v'' = 0$; frequencies in cm^{-1}. [b] Tabulated absorbance values have been multiplied by 10^5.

is shown in ref 25 and illustrated by example in ref 26. Standard notion, with quantities pertaining to the ground state indicated by a double prime and those for the excited state by a single prime, is adopted below.

For the $X^2\Pi$ state ($\Lambda = \pm 1$, $S = 1/2$), for any given vibrational level the rotational levels (aside from Λ-type doubling) are found from a 2×2 matrix[27] with diagonal elements given by:

$$B[(J+S)^2 - \Lambda^2)] \pm 1/2(A - 2B) \qquad (1)$$

and off-diagonal elements by $B[(J+S)^2 - \Lambda^2]^{1/2}$, where J is the total angular momentum, B is the rotational constant, and A is the spin−orbit coupling constant. Levels associated with the plus sign in eq 1 are denoted F_2, those with the minus sign F_1; in the pure Hund's Case (a) limit, approached at low J, these correspond to the $^2\Pi_{1/2}$ and $^2\Pi_{3/2}$ components, respectively. For NaO, the Λ-type doubling term for the $^2\Pi_{1/2}$ state is unusually large,[17] approximately 0.05 $(J + S)$ cm^{-1}, and thus it was included in the simulation. Centrifugal distortion and other high-order terms were neglected.

TABLE 4: Observed NaO Absorption Lines, $\Delta v = +1$ Band[a]

frequency	absorbance[b]	frequency	absorbance[b]
2646.553	5.70	2656.536	2.23
49.123	5.11	56.584	1.80
49.280	2.66	56.805	3.30
49.343	1.99	58.135	4.32
49.961	2.47	58.210	7.66
50.318	2.31	58.321	6.30
50.474	6.20	58.604	7.78
50.521	5.46	59.480	3.51
50.624	7.90	60.164	3.17
51.206	4.10	60.189	3.64
51.388	3.40	63.823	4.02
52.394	2.38	63.978	4.99
52.776	4.60	64.523	2.88
52.903	2.72	66.058	4.77
53.306	2.98	66.362	6.30
53.417	3.46	66.962	10.2
54.356	10.2	67.073	3.93
54.422	3.06	78.416	3.20
54.496	5.96	91.369	2.55
54.670	5.46	96.134	3.32
55.450	4.02	96.162	2.89
56.098	3.85	96.576	2.53
56.448	6.01		

[a] $A^2\Sigma^+ \leftarrow X^2\Pi$, $v'-v'' = 1$; frequencies in cm^{-1}. [b] Tabulated absorbance values have been multiplied by 10^5.

For the $A^2\Sigma^+$ state ($\Lambda = 0$, $S = 1/2$), Hund's Case (b) applies and the rotational levels[27] are given by:

$$BN(N+1) + E_{sr} \qquad (2)$$

where N is the total angular momentum excluding electronic spin and E_{sr}, the spin-rotation term, is given by $1/2\gamma N$ and $-1/2\gamma(N+1)$ for the F_1 levels (with $N = J - 1/2$) and F_2 levels (with $N = J + 1/2$), respectively. For the spin-rotation constant, we used a nominal estimate, $\gamma = 0.01$ cm^{-1}.

The selection rules[25] are $+ \leftrightarrow -$ for parity and $\Delta J = 0, \pm 1$; these allow 12 rotational branches, designated Q_{11}, Q_{12}, Q_{21}, Q_{22}, and similarly for P and R branches. Here, for example, the subscript "12" designates a $F_1' \leftarrow F_2''$ transition. For NaO, because the ratio A/B is large ($\sim 107/0.4 \approx 250$), low J transitions with $\Delta J \neq \Delta N$, which are forbidden in the absence of spin−orbit coupling, are not much weaker than those with $\Delta J = \Delta N$.

As a check of the Hamiltonian and our computer program, we generated frequencies for an analogous $^2\Pi - ^2\Sigma^+$ band system for SiN and found good agreement with the observed spectrum.[26]

Intensities. The intensities were evaluated from the rotational line strengths[28,29] and the absorption cross sections of the vibronic bands. The latter cross sections[30] are given by:

$$(8\pi^2)^{-1} f_e f_v f_R (1 - e^{-u})(c^2/\nu^2) A_{v'v''}/\Delta\nu \qquad (3)$$

where the f's are the fractional electronic, vibrational, and rotational populations of the lower state, ν is the transition frequency, $\Delta\nu$ is the Doppler line width, and $A_{v'v''}$ is the Einstein A coefficient. The factor containing $u = h\nu/k_B T$ takes account of stimulated emission from a thermal population of the A state.

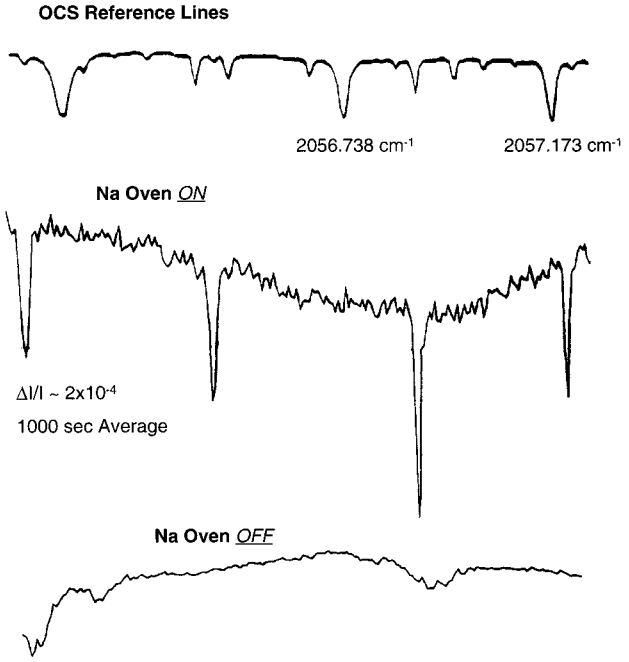

Figure 2. High-resolution spectrum of NaO. These are some of the strongest transitions near ~2056 cm^{-1}, with an absorbance of $DI/I \sim 2 \times 10^{-4}$. The upper trace shows the OCS reference lines used to calibrate the frequency position. The middle and lower traces are scans when the sodium oven was hot and cold, respectively. The spectrum was recorded with signal averaging over 1000 s.

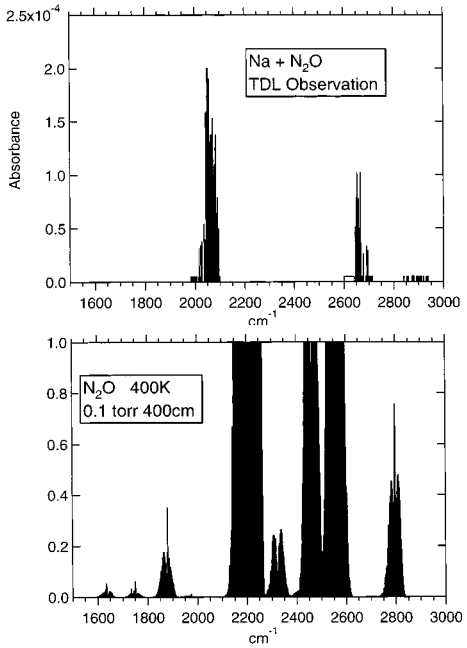

Figure 3. Observed spectra attributed to NaO (upper plot) and N_2O (bottom plot) bands from HITRAN 96 data file.

Of course, if the Na + N_2O reaction produces NaO(A) directly (as possibly indicated by ref 10) and the chemically produced NaO(A) is not collisionally quenched under our experimental conditions, then eq 3 is insufficient. The Boltzmann factors were evaluated for $T = 460$ K, with vibrational frequencies from ref 15 and rotational constants from ref 17. The $A_{v'v''}$ coefficients used, listed in Table 1, were computed by Langhoff.[16]

Results and Discussion

A total of 109 absorption lines from 2015.440 to 2095.418 cm^{-1} (Table 3) and 45 lines from 2646.553 to 2696.576 cm^{-1}

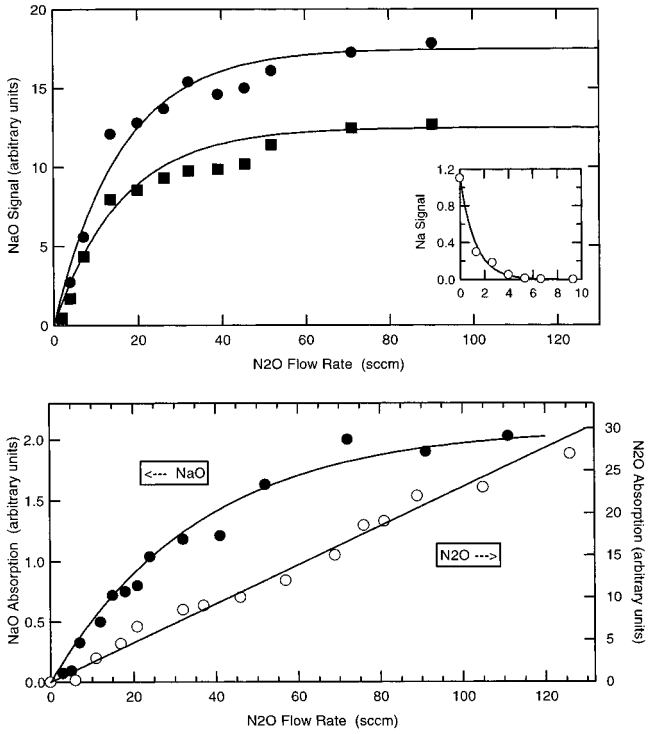

Figure 4. Summary of kinetic tests to confirm NaO radical observations. The upper panel plots NaO line intensity versus N_2O flow rate. Data are shown for two different NaO absorption lines (□) and (○). The inset plots the first-order decay of the atomic Na fluorescence signal. The curves fitted to data points have the form: $S_{N_2O} = S_1(1 - \exp k_1[N_2O])$ and $S_{Na} = S_2(\exp k_2[N_2O])$. The observed ratio, $k_1/k_2 = 13$, is in accord with the ratio of the distance from the sodium oven to the PMT (~90 cm) to that from the diode laser beam to the sodium oven (~7 cm). The saturation of the signal for N_2O flow rates greater than ~35 sccm, as predicted by the kinetic model, is consistent with the absorption by NaO from the Na + N_2O reaction. The lower panel compares NaO and N_2O absorptions as a function of the N_2O flow rate. The NaO signal saturates, as above, while the N_2O absorption is linear with added N_2O. NaO saturates at higher N_2O flow than above, since in the lower panel the flow tube was operated at lower total pressure (1 Torr below versus 3 Torr above), again consistent with Na + N_2O reaction kinetics.

(Table 4) attributed to NaO were measured with an accuracy of ~0.005 cm^{-1}. Typical absorption features from the 2000−2100 cm^{-1} ($\Delta v = 0$) region are shown in Figure 2 along with OCS reference scans. Spectral line absorbances were determined by signal averaging for 1000 s; typically these were of the order $\Delta I/I \sim 10^{-4}$. The lines attributed to NaO disappeared when the sodium flow was interrupted. As expected many other strong lines due to N_2O were observed. As seen in Figure 3, the NaO lines observed were found in spectral regions unobscured by the precursor N_2O lines.

Figure 4 shows results of kinetic experiments performed to confirm the identity of the NaO lines. Since the N_2O flow was injected in excess, the NaO signal intensity was not proportional to the N_2O flow rate, while N_2O lines were almost linearly dependent upon N_2O flow rate. The intensity of the NaO signal did decrease when the N_2O flow rate was decreased below the Na flow. First-order decay of the Na vapor fluorescence signal was also observed as the N_2O flow was increased. The NaO signal versus N_2O flow rate could be enhanced by varying the total pressure and other flow conditions (Figure 4). The Na + N_2O reaction is expected to produce a mixture of X and A state NaO;[10] thus at higher pressure or slower flow rates the excited NaO $A^2\Sigma$ state may be deactivated to the $X^2\Pi$ state by radiative or physical quenching.

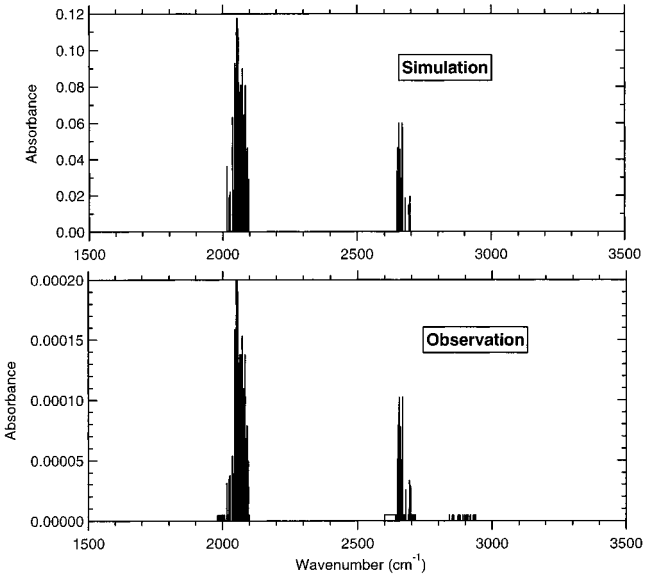

Figure 5. Comparison of the NaO $A^2\Sigma^+ \leftarrow X^2\Pi$ band simulation (upper plot) and the actual observation (lower plot). Stick spectra are shown for the $\Delta v = 0$ band in the 2015−2095 cm^{-1} region and the $\Delta v = +1$ band in the 2646−2697 cm^{-1} region. Lines appearing in frequency intervals not covered by the diode laser scans are omitted.

Figure 5 compares the observed NaO lines for the $\Delta v = 0$ and $\Delta v = 1$ regions with our band simulations (described above) based on the ab initio calculations by Langhoff and coworkers.[15,16] For this comparison, lines falling within the many gaps due to the limited coverage obtainable with available diode lasers (see Appendix) were deleted from the simulations. The net frequency coverage attained for the $\Delta v = 0$ and $\Delta v = 1$ wavenumber regions was only about 30−35%. We also added 75 cm^{-1} to the ab initio frequencies, to obtain the best match between the observed and simulated spectra; this produced rather good overall agreement. Our efforts to examine the $\Delta v = 2$ region near ∼2900−3050 cm^{-1} proved fruitless because available diode lasers performed very poorly there.

The strongest $\Delta v = 0$ lines (2050−2060 cm^{-1}) of NaO showed absorbances of $\sim 2 \times 10^{-4}$ after signal averaging for ∼1000 s (Figure 2). However, the observed intensity was about 100 times weaker than expected. From Beer's Law small absorbances can be represented by:

$$\Delta I/I = N_{\mathrm{NaO}} \sigma_{21} l \qquad (4)$$

where N_{NaO} is the sodium oxide number density, σ_{21} is the absorption cross section, and l is the optical path length. For our apparatus, the multipass path length is estimated to be $l \sim$ 100 cm. The absorption cross section was calculated to be $\sigma_{21} \sim 10^{-16}$−$10^{-17}$ cm^2 for the strongest $\Delta v = 0$ transitions using Langhoff's Einstein coefficients (Table 1). The NaO number density was estimated as 10^{12}−10^{14} cm^{-3} for an initial sodium vapor pressure of $> 10^{-3}$ Torr, producing an expected absorbance range between 10^{-3} and ∼1. Of course, some wall loss of Na and NaO is expected; however, our experience with the kinetics of these species suggests that these losses will not be extensive over the short flow distance between the NaO production and observation regions. Langhoff's Einstein A coefficient calculations[16] may be overestimates; calculations mentioned in ref 17 indicate somewhat smaller values. Also, since the Na + N_2O reaction is believed to produce NaO in both the $A^2\Sigma$ and $X^2\Pi$ states,[10] an unknown fraction of the NaO produced may remain in the excited state reducing the absorbance.

TABLE 5: Assigned NaO Lines, 0−0 Band[a]

branch (J'')	ν_{obs}, cm^{-1}	$\nu_{\mathrm{obs}}-\nu_{\mathrm{cal}}$, cm^{-1}	intensity
$Q_{11}(12.5)$	2049.489	0.001	12.3
$Q_{11}(13.5)$	2050.240	0.003	8.30
$Q_{11}(14.5)$	2051.086	0.003	12.0
$Q_{11}(15.5)$	2052.044	0.0040	17.8
$Q_{11}(16.5)$	2053.034	0.026	12.1
$Q_{11}(19.5)$	2056.512	−0.004	11.4
$Q_{21}(4.5)$	2050.097	0.001	3.00
$Q_{21}(7.5)$	2052.824	0.011	20.0
$Q_{21}(10.5)$	2056.261	−0.015	11.4
$Q_{21}(11.5)$	2057.597	0.000	2.38
$P_{21}(5.5)$	2045.499	0.032	10.4
$R_{11}(6.5)$	2053.290	0.018	20.0
$R_{11}(11.5)$	2060.041	0.032	2.75
$R_{11}(15.5)$	2066.898	0.008	4.31

[a] The calculated frequencies were obtained using for the $X^2\Pi$ data the parameters listed in Table 2 and for the $A^2\Sigma^+$ state $B' = 0.462$ cm^{-1}, $D' = 1.30 \times 10^{-6}$ cm^{-1} (centrifugal distortion), and $\gamma = 0.193$ cm^{-1} (spin-rotation), with $T_{0-0} = 1992.905$ cm^{-1} (band origin).

A spectral analysis is in progress which will help provide a better understanding of the molecular structure and interatomic potential of the NaO radical. To date 14 lines have been assigned, as displayed in Table 5. This assignment is based on the ground-state combination differences which were previously determined from the microwave spectrum of NaO.[17] These pairs are $Q_{11}(J''+1)-R_{11}(J'')$ for $J'' = 11.5$ 15.5; and $P_{21}(J''+1)-Q_{21}(J'')$ for $J'' = 4.5$. Among the 14 assigned lines, 3 pairs (6 lines) are matched with the ground-state combination differences. Other assignments are based chiefly on the recognition that the Q_{11} branch would have strong transitions and aided by the fact that it is simpler to fit Q_{11} with polynomial terms than the other branches. To compute frequencies for comparison with the assigned lines (Table 5), several higher order terms that had been neglected in the preliminary simulations were added to the Hamiltonian. For the $^2\Pi$ states, the diagonal terms of eq 1 were replaced by:

$$Bx^2 - D(x^4 + x^2 - 1) + 1/2(1 \mp x)p + 1/2(1 \mp x)^2 q - 1/2A \quad (5a)$$

$$B(x^2 - 2) - D(x^4 - 3x^2 + 3) + 1/2(x^2 - 1)q + 1/2A \quad (5b)$$

for the F_1 and F_2 components, respectively, where $x = J + 1/2$; D is the centifugal distortion constant, and p and q are the lambda-doubling parameters. The off diagonal elements of eq 2 were replaced by:

$$B(x^2 - 1)^{1/2} + 2D(x^2 - 1)^{3/2} - 1/4(x^2 - 1)p - 1/2(1 \pm x)(x^2 - 1)^{1/2} q \quad (6)$$

For the $^2\Sigma^+$ state, a centrifugal distortion term, $-DN_2(N+1)_2$, was added to eq 3.

$$BN(N+1) - DN^2(N+2)^2 + E_{\mathrm{sr}} \qquad (7)$$

The NaO($A^2\Sigma^+$) molecular constants (in cm^{-1}) corresponding to these assignments are T_{0-0} (band origin) = 1992.905; B' (rotational) = 0.462; D' (centrifugal) = 1.30×10^{-6}; γ' (spin-rotation) = 0.193. The first two values agree quite well with those calculated by Langhoff et al.[15] who predicted $T_{0-0} = 1918$ cm^{-1} and $B' = 0.467$−0.470 cm^{-1}. The large derived spin-rotation constant (19 times larger than assumed in the spectral simulation parameters shown in Table 2) may be due to the small energy difference between the $X^2\Pi$ and $A^2\Sigma^+$ states.

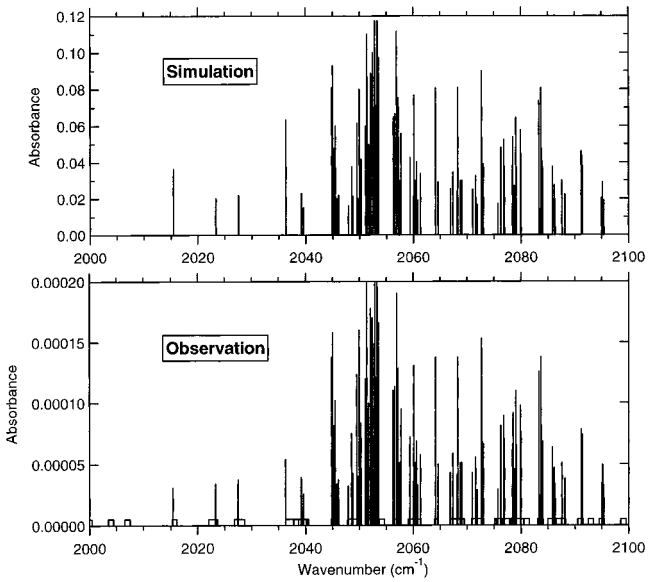

Figure 6. Spectral simulations with higher order Hamiltonian terms and preliminary $A^2\Sigma^+$ molecular constants derived from the observed spectra compared with the obervations. Spectra and frequency interval are as for the $\Delta v = 0$ band in Figure 5.

Repeating the spectral simulations including the higher order terms in the Hamiltonian and the $^2\Sigma^+$ molecular constants derived from the assignments was found not to appreciably affect the band profile shape, as plotted in Figure 6 for the $\Delta v = 0$ region.

The direct observation of the $A^2\Sigma^+ \leftarrow X^2\Pi$ transition of NaO reported here has several interesting implications for the chemistry of the mesospheric sodium nightglow and related laboratory chemical kinetics studies. First, the lower than expected absorbance noted above indicates that the radiative lifetime of NaO($A^2\Sigma^+$) is longer than the 10−30 ms calculated by Langhoff et al.[16] and possibly significantly longer than the 10−100 ms NaO chemical lifetime set by the NaO + O reaction in the 85−95 km region of the mesosphere.[33] In addition, our observations probably indicate that physical quenching of NaO($A^2\Sigma^+$) by He, Ar, and N_2O in our flow tube is slow, suggesting that quenching by the major atmospheric gases N_2 and O_2 will also be slow. Thus, our observations lend credence to the suggestion that the NaO($A^2\Sigma^+$) has a sufficiently long atmospheric lifetime that it can efficiently serve as the chain carrier for Na(^{2}P) production in the mesosphere.[11,33]

Furthermore, since most laboratory kinetic studies of NaO kinetics have used the Na + N_2O reaction as a convenient laboratory reactant source, their measured rate constants correspond to either nearly pure $X^2\Pi$ state kinetics for high-pressure experiments[4] or mixed $A^2\Sigma^+/X^2\Pi$ state kinetics for low-pressure experiments.[33,34] Neither may be representative of mesospheric NaO resulting in some error in current models of the mesospheric sodium layer and nightglow. Fortunately, the identification of NaO $A^2\Sigma^+ \leftarrow X^2\Pi$ transitions opens up the possibility of laser pump/probe experiments which should allow the determination of accurate radiative decay, physical quenching, and chemical reaction lifetimes (rate constants) for NaO($A^2\Sigma^+$) prepared by laser excitation of NaO($X^2\Pi$).

Acknowledgment. We thank Sang-Woon Yoon for experimental assistance in the early stages of this work, Prof. R. W. Field for helpful correspondence, and Dr. S. R. Langhoff for kindly supplying his unpublished ab initio calculations of NaO band origins and transition probabilities. S.K.K. is grateful to the Seoam Foundation for a Visiting Fellowship at Harvard University. We also gratefully acknowledge the financial support of the Atmospheric Sciences Division of the National Science Foundation under Grant No. 9304528.

Appendix: Regions Scanned

Listed here are the frequency intervals (in cm^{-1}) in which our diode lasers enabled spectral scans with fair to good sensitivity. For example, the first listed interval exends from 1981.5 to 1982.5 cm^{-1}. The three groups (I, II, III) correspond to regions containing the 0−0, 1−0, and 2−0 vibronic bands of NaO.

I	II	III
1981.5−1982.5	2645.7−2646.6	2840.2842.
1997.5−1998.4	2649.1−2649.9	2852.2854.
1999.5−2000.5	2649.5−2651.9	2854.2−2856.9
2015.3−2016.2	2652.2−2655	2874.5−2876.9
2022.1−2023.7	2654.9−2656.8	2877.9−2878.1
2026.8−2028.7	2658.1−2659.9	2878.4−2880.7
2036.3−2040.5	2663.3−2665.	2897.9−2898.1
2044.8−2046.2	2666.4−2667.8	2890.9−2891.1
2047.8−2050.4	2678.3−2678.5	2904.9−2905.1
2051.1−2052.2	2691.2−2692.	2905.9−2906.1
2052.35−2054.6	2695.7−2697.1	2910.9−2911.1
2056.2−2057.8		2918.9−2919.1
2059.1−2061.4		2930.9−2931.1
2063.9−2064.62		2931.9−2932.1
2067.2−2069.5		2932.9−2933.1
2070.9−2073.1		2935.9−2936.1
2075.1−2080.5		2937.9−2938.1
2083.05−2084.05		2952.9−2953.1
2084.9−2088.2		2955.9−2956.1
2091.−2092.		
2093.−2094.		
2095.−2096.5		

References and Notes

(1) Chapman, S. *Astrophys. J.* **1939**, *90*, 309.
(2) Kolb, C. E.; Elgin, J. B. *Nature* **1976**, *263*, 488.
(3) Bates, D. R.; Ojha, P. C. *Nature* **1980**, *286*, 790.
(4) Plane, J. M. C.; Husain, D. *J. Chem. Faraday Trans. II* **1986**, *82*, 2047.
(5) Schofield, K. *Geophys. Res. Lett.* **1993**, *20*, 2837.
(6) Schofield, K. *Int. J. Chem. Kinet.* **1993**, *25*, 719.
(7) Helmer, M.; Plane, J. M. C. *J. Geophys. Res.* **1993**, *98*, 23207.
(8) Clemesha, B. R.; Simonich, D. M.; Takahashi, H.; Melo, S. M. L.; Plane, J. M. C. *J. Geophys. Res.* **1995**, *100*, 18909.
(9) Shi, X.; Herschbach, D. R.; Worsnop, D. R.; Kolb, C. E. *J. Phys. Chem.* **1993**, *97*, 2113.
(10) Wright, T. G.; Ellis, A. M.; Dyke, J. M. *J. Chem. Phys.* **1993**, *98*, 2891.
(11) Herschbach, D. R.; Kolb, C. E.; Worsnop; Shi, X. *Nature* **1992**, *356*, 414.
(12) Allison, J. N.; Goddard, W. A., III. *J. Chem. Phys.* **1982**, *77*, 4259.
(13) Allison, J. N.; Cave, R. J.; Goddard, W. A., III. *J. Phys. Chem.* **1984**, *88*, 1262.
(14) Langhoff, S. R.; Bauschlicher, C. W., Jr.; Partridge, H. *J. Chem. Phys.* **1986**, *84*, 4474.
(15) Langhoff, S. R.; Partridge, H.; Bauschlicher, C. W., Jr. *Chem. Phys.* **1991**, *153*, 1.
(16) Langhoff, S. R. Private communication.
(17) Yamada, C.; Fujitake, M.; Hirota, E. *J. Chem. Phys.* **1989**, *90*, 3033.
(18) Pfeifer, J.; Gole, J. L. *J. Chem. Phys.* **1984**, *80*, 565.
(19) Pugh, J. V.; Shen, K. K.; Winstead, C. B.; Gole, J. L. *Chem. Phys.* **1996**, *202*, 129.
(20) Murad, E.; Swider, W.; Benson, S. W. *Nature* **1981**, *289*, 273.
(21) Lamb, J. J.; Benson, S. W. *J. Geophys. Res.* **1986**, *91*, 8683.
(22) Worsnop, D. R.; Zahniser, M. S.; Kolb, C. E. *J. Phys. Chem.* **1991**, *95*, 3691.
(23) Worsnop, D. R.; Nelson, D. D.; Zahniser, M. S. *SPIE Proc.* **1992**, *1715*, 18.
(24) Nelson, D. D.; Zahniser, M. S.; McManus, J. B.; Shorter, J. H.; Wormhoudt, J. C.; Kolb, C. E. *SPIE Proc.* **1996**, *2834*, 148.

(25) Herzberg, G. *Molecular Spectra and Molecular Structure, I. Spectra of Diatomic Molecules*; van Nostrand Reinhold Co.: New York, 1950. See Figure 123, p 259, for an energy level diagram indicating allowed transitions for a $^2\Pi-^2\Sigma^+$ band.
(26) Yamada, C.; Hirota, E.; Yanamoto, S.; Saito, S. *J. Chem. Phys.* **1988**, *88*, 46.
(27) Zare, R. N. *Angular Momentum*; Wiley-Interscience: New York, 1988.
(28) Hill, E. L.; Van Vleck, J. H. *Phys. Rev.* **1928**, *32*, 250.
(29) Earl, L. T. *Phys. Rev.* **1935**, *48*, 423.
(30) Penner, S. S. *Quantitative Molecular Spectroscopy and Gas Emissivities*; Addison-Wesley Publishing Co.: Reading, MA, 1959.
(31) Mead, R. D.; Hefter, U.; Schulz, P. A.; Lineberger, W. C. *J. Chem. Phys.* **1985**, *82*, 1723.
(32) Kotlar, A. J.; Field, R. W.; Steinfeld, J. I. *J. Mol. Spectrosc.* **1980**, *80*, 86.
(33) Kolb, C. E.; Worsnop, D. R.; Zahniser, M. S.; Robinson, G. N.; Shi, X.; Herschbach, D. R. In *Gas-Phase Metal Reactions;* Fontijn, A., Ed.; Elsevier Science Publishers: Amsterdam, 1992; p 15.
(34) Ager, J. W., III; Howard, C. J. *J. Chem. Phys.* **1987**, *87*, 921.